

PAPER

Valence band states in an InAs/AlAsSb multi-quantum well hot carrier absorber

To cite this article: V R Whiteside *et al* 2019 *Semicond. Sci. Technol.* **34** 025005

View the [article online](#) for updates and enhancements.

Recent citations

- [Detailed balance calculations for hot-carrier solar cells: coupling high absorptivity with low thermalization through light trapping](#)
Maxime Giteau *et al*
- [The role of intervalley phonons in hot carrier transfer and extraction in type-II InAs/AlAsSb quantum-well solar cells](#)
V R Whiteside *et al*



IOP | ebooks™

Bringing together innovative digital publishing with leading authors from the global scientific community.

Start exploring the collection—download the first chapter of every title for free.

Valence band states in an InAs/AlAsSb multi-quantum well hot carrier absorber

V R Whiteside^{1,6}, B A Magill^{2,6}, Matthew P Lumb^{3,4}, H Esmailpour¹, M A Meeker², R R H H Mudiyansele², A Messenger⁵, S Vijayaragunathan¹, T D Mishima¹, M B Santos¹, I Vurgaftman³, G A Khodaparast^{2,7} and I R Sellers^{1,7}

¹ Department of Physics & Astronomy, University of Oklahoma, Norman, OK 73019, United States of America

² Department of Physics, Virginia Tech, Blacksburg, VA 24061, United States of America

³ U.S. Naval Research Laboratory, Washington, DC 20375, United States of America

⁴ George Washington University, Washington, DC 20037, United States of America

⁵ Laboratoire des Solides Irradiés, CNRS UMR 7642, CEA-DSM-IRAMIS, École polytechnique, Université Paris-Saclay, F-91128 PALAISEAU cedex, France

E-mail: khoda@vt.edu and sellers@ou.edu

Received 12 April 2018, revised 27 August 2018

Accepted for publication 27 September 2018

Published 7 January 2019



CrossMark

Abstract

In this study, detailed temperature dependent simulations for absorption and photogenerated recombination of hot electrons are compared with experimental data for an InAs/AlAsSb multi-quantum well. The simulations describe the actual photoluminescence (PL) observations accurately; in particular, the room temperature e1-hh1 simulated transition energy of 805 meV closely matches the 798 meV transition energy of the experimental PL spectra, a difference of only 7 meV. Likewise, the expected energy separations between local maxima (p1–p2) in the simulated/experimental spectra have a difference of just 2 meV: a simulated energy separation of 31 meV compared to the experimental value of 33 meV. Utilizing a non equilibrium generalized Planck relation, a full spectrum fit enables individual carrier temperatures for both holes and electrons. This results in two very different carrier temperatures for holes and electrons: where the hole temperature, T_h , is nearly equal to the lattice temperature, T_L ; while, the electron temperature, T_e , is ‘hot’ (i.e., $T_e > T_L$). Also, by fitting the experimental spectra via three different methods a ‘hot’ carrier temperature is associated with *electrons only*; all three methods yield similar ‘hot’ carrier temperatures.

Keywords: hot carriers, type-II band alignment, valence band states, photovoltaics

(Some figures may appear in colour only in the online journal)

Photovoltaic solar cells are considered an established technology [1] as a source of clean energy; therefore, any increase in the efficiency in solar cells is likely to have immediate and profound dividends. One limitation of photovoltaic cells is that excess energy (i.e., any energy above the band gap of the material) in photogenerated carriers is typically lost through efficient carrier thermalization. This process is dominated by

the emission of longitudinal optical (LO) phonons that decay into two Klemens phonons [2, 3]. This thermalization of excited carriers is one of the major contributing factors [4] that limits the efficiency of photovoltaic cells to $\sim 30\%$ [5].

One solution for this problem is to construct multi-junction devices. Presently, the world record power conversion efficiency is 38% at 1 sun [6] but, this is expensive and has seen limited commercial terrestrial usage. An alternative solution is to design devices to minimize the energy lost to phonons. A promising example for this class of devices, is a ‘hot-carrier’

⁶ Authors with equal contributions.

⁷ Authors to whom any correspondence should be addressed.

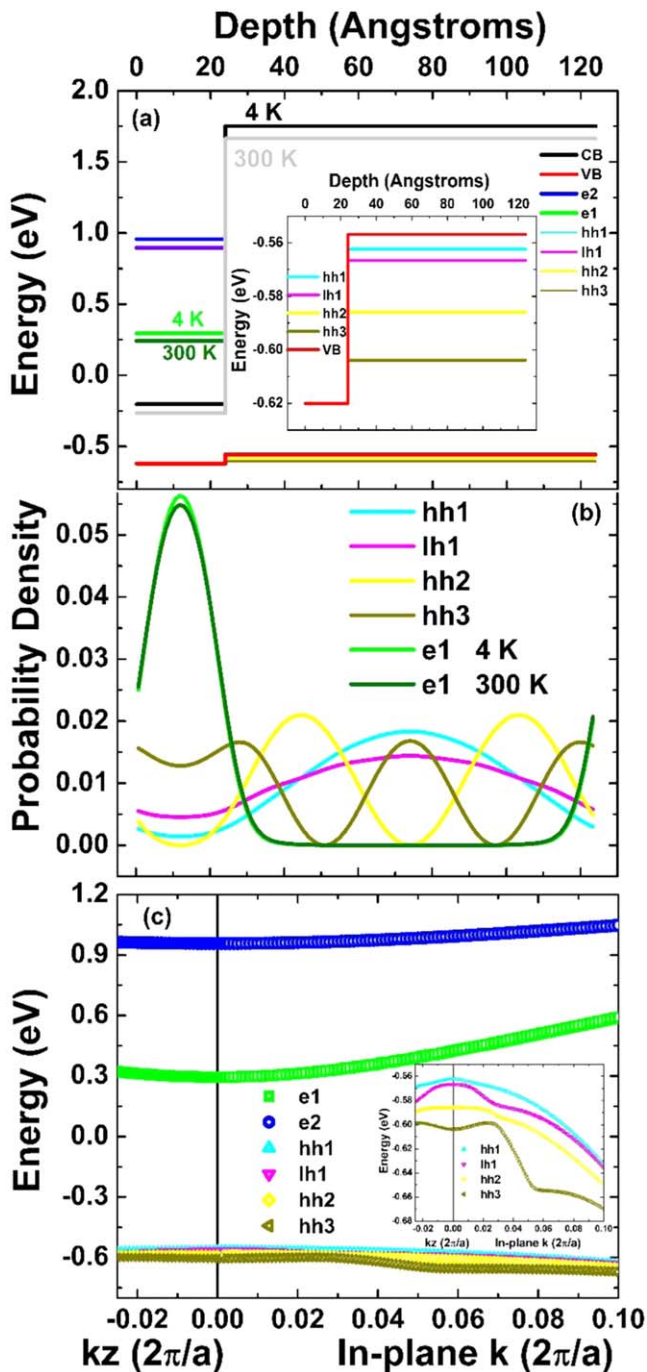


Figure 1. (a) The temperature dependent (4–300 K) band structure of a single InAs/AlAsSb QW with associated confined energies and (b) probabilities of 2 lowest electron and 4 lowest hole wavefunctions. Inset to (a) is an expanded view of the valence band. (c) The energy dispersion of the 2 lowest electron levels and 4 lowest hole levels; the inset is an expanded view of the valence band dispersion, where the structure at higher k values is clearly seen.

solar cell, where the excited carriers are extracted before they lose all of their excess energy to their surroundings.

To construct a photovoltaic device to take advantage of ‘hot-carriers’, two underlying principles that have been pursued in the design of a prototypical hot carrier solar cell (HCSC) are: first, the HCSC needs to be engineered such that e.g., the emitted phonons live longer than the hot carriers in

order to increase the hot carrier density through re-absorption of phonons by the carriers [7] or the cooling process is inhibited [8–11]. Second, the contacts to the device need to function over a narrow energy range [12–14], covering only a limited portion of the distribution of hot carriers; this allows for the collection of hot carriers, while restricting the ability of the excited carriers to reach thermal equilibrium through the contacts [15].

Several investigations of hot carrier absorbers have introduced reduced dimensionality [9–11, 13, 16, 17] into the device design in order to take advantage of the extended phonon lifetimes [9–11] that have been previously observed in quantum well structures [9–11] as compared to bulk materials. A seemingly straight forward generalized Planck relation analysis of the high energy portion of the photoluminescence (PL) spectra following LeBris *et al* [10] has been applied by several groups [9, 10, 18–23] to determine a ‘hot’ carrier temperature. Full spectrum fits have been employed to evaluate the electron and hole quasi-Fermi level splitting [24–26] and single carrier temperature [27, 28]. Recently, Gibelli *et al* have applied a full spectrum fit of the PL spectra to extract the individual ‘hot’ carrier temperatures for both: holes and electrons [29].

Another aspect of evaluating a material as a suitable hot carrier absorber is determining a Q-factor [10], which is a measure of how efficient the phonon–electron interaction is in thermalizing ‘hot’ carriers back to the ambient (lattice) temperature. The applicability of this method to structures with type-II band alignments is not clear—especially, at elevated temperatures due to the lack of excitation power dependence of the temperature difference between the carriers (T_c) and lattice (T_L). This has been observed previously in the multi-quantum well (MQW) structure that is being investigated here [30].

One critical issue has been the treatment of additional confined (resonant) states that occur with reduced dimensionality [31] causing complications in the analysis of the hot carrier temperature [32]. When the majority of the absorbed photon’s energy is transferred primarily (due to a large difference in effective mass of electrons and holes) to the photoexcited electron and not the hole, the discussion has centered around the confined electron states. InAs is a case in point where there is a large difference in effective masses ($m_h \gg m_e$) [33]. However, one should not discount the valence band (VB) states and their role/effect just because the majority of the energy is transferred to the electron.

In this study, the proposed ‘hot’ carrier absorber structure is comprised of 30 InAs quantum wells that are 2.4 nm thick with 10 nm thick AlAs_{0.16}Sb_{0.84} barrier layers; the composition is such as to be lattice matched to InAs, the growth conditions have been described previously [18]. To only probe the ‘hot carrier’ absorber material, the substrate, buffer layer, and cap layer were all removed through a combination of mechanical polishing and selective etchants, a more thorough description of the process has been published elsewhere [34].

Band structure calculations for the periodic well/barrier system have been carried out using the Naval Research

Laboratory's (NRL) MultiBands[®] software tool [35] which employs an 8-band k-p model, including temperature and strain dependent band parameters adopted from Vurgaftman *et al* [36]. The absorption and recombination spectra for the interband transitions between the lowest energy electron sub-band and the lowest four hole sub-bands are computed from the superlattice band structure and optical matrix elements. A computationally efficient interpolation algorithm, described in [35], was used to accomplish this. A Gaussian broadening of 5 meV was applied to each absorption spectrum. This paper will provide details on the simulations as well as compare the results to experimental data.

As the most interesting/complicated experimental results occur at elevated temperatures/high power, the experimental results will be limited to $T \geq 150$ K. The PL was measured using a 20× Mitutoyo near infrared microscope objective lens in combination with a liquid nitrogen (LN₂) cooled Linkam THMS600e cryostat coupled into an Acton 2500i spectrometer with a LN₂ cooled linear InGaAs array or a 270M Spex spectrometer with a LN₂ cooled Germanium detector. The excitation source was either the 632.8 nm line of a He-Ne laser or the 1064 nm line of a solid state diode laser.

While our previous studies have shown hot carrier temperatures at elevated temperatures due to the delocalization of holes, the question remains as to what level do the multiple VB states effect the 'hot' carrier temperature. In order to more fully evaluate this question a series of simulations have been performed to model the temperature dependence of the absorption and recombination of the 30 MQW InAs/AlAsSb structure that has been proposed as a 'hot' carrier absorber.

Figure 1(a) shows the temperature dependent contraction of the conduction band (CB) from 4 K (black) to 300 K (gray) and the negligible contraction of the VB from 4 to 300 K (red) for a single quantum well; as well as, the first (4 K, green; 300 K, dark green) and second (4 K, blue; 300 K violet) confined electron states: e1 and e2, respectively. The inset shows an expanded view of the VB to clearly see the first four hole levels. There is a 31 meV separation between the first and fourth confined hole states.

For simulation purposes, the direct band gap (2.2 eV, $T = 300$ K) of AlAsSb is used because the CB well is formed by the two CB minima at the gamma point, so the well depth in the CB is defined by the AlAsSb gamma CB valley; the lower energy (1.6 eV, $T = 300$ K) indirect band gap would provide little or no absorption for an indirect absorption due to the relatively thin layer (10 nm). The conduction band offset is calculated to be 1.95 eV at 4 K with a 25 meV contraction at room temperature. The VB offset (VBO) is calculated to be 63 meV at 4 K with less than a 1 meV contraction at 300 K. At 4 K and $k_z = 0$, the energy separation for e1-hh1 transition is 857 meV, for e1-e2 it is 685 meV, and the hole state separation hh1-hh3 is 31 meV.

The large e1-e2 separation limits any thermal occupation of the resonant e2 state as $k_B T$ at room temperature is only 26 meV; contrasting this with the hole state occupation, $k_B T$ at room temperature is of the same order as the hole separation for *all* of the lowest four hole states. While there is an extremely small temperature dependence for VB states

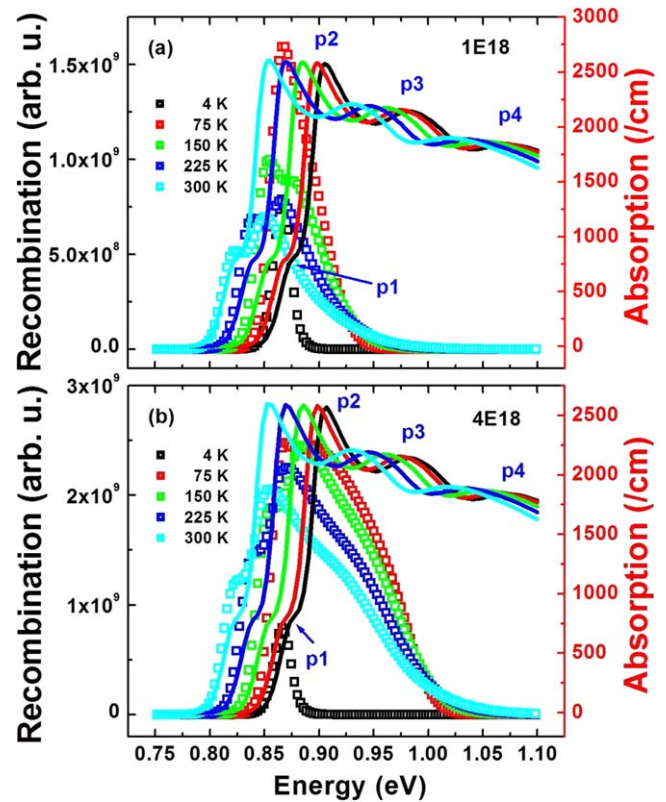


Figure 2. (a) Simulated absorption for select temperatures (4 K, black line; 75 K, red; 150 K, green; 225 K, blue; 300 K, cyan; right axis). Simulated recombination of photogenerated carriers with a carrier density of $1 \times 10^{18} \text{ cm}^{-3}$ (4 K carrier density is $4 \times 10^{17} \text{ cm}^{-3}$ for computational reasons) for select temperatures (open symbols, left axis). (b) Simulated absorption for select temperatures (4 K, black line; 75 K, red; 150 K, green; 225 K, blue; 300 K, cyan; right axis). Simulated recombination of photogenerated carriers with a carrier density of $4 \times 10^{18} \text{ cm}^{-3}$ (4 K carrier density is $4 \times 10^{17} \text{ cm}^{-3}$ for computational reasons) for select temperatures (open symbols, left axis).

~ 1 meV, the confined electron levels contract 52 meV over the whole temperature range, such that the room temperature (300 K) e1-hh1 energy separation is 805 meV.

The probability density of the wavefunctions for electrons (e1: green 4 K and olive 300 K; e2 not shown for clarity) and first 4 hole wavefunctions (hh1 cyan, lh1 magenta, hh2 yellow, hh3 brown, respectively) are plotted in figure 1(b). There is considerable penetration into the respective barriers ~ 10 nm for the electron into the AlAsSb barrier (~ 20 nm total); only hh2 goes to zero in the center of the InAs QW where the 'bounding' node (for a well confined wavefunction) would be pushed into. The other three hole wavefunctions show a nonzero minimum, especially hh3.

At finite temperatures due to the small separation of hole states there is a finite occupation of the more energetic hole states (lh1, hh2, hh3) which is dependent on carrier concentration (see figure 2). Additionally, there is a mixing of VB states due to the MQW structure actually forming minibands at each of the simulated hole levels. This causes a relaxation of optical selection rules such that a normally dark transition (e1-hh2) is no longer strictly forbidden.

The simulation is based on sp^3 hybridization, where states that have a greater percentage s -like and p_z -like characteristics belong to the light hole band; similarly states that have a more p_x , p_y -like characteristics are assigned to the heavy hole band. Based on simulation results, the hh1, hh2, and hh3 hole states all have more p_x , p_y -like characteristics than s -like and p_z -like characteristics and are classified as heavy hole states; while the lh1 state has a stronger s -like and p_z -like characteristics compared to the other three VB states and is classified as the lowest energy state for light hole VB, lh1. The transition e1-lh1 would be an allowed transition from the lowest energy state of the light hole band to the lowest electron confined level e1.

Without mixing (relaxation of optical selection rules) then, the only strictly forbidden transition would be e1-hh2, this transition corresponds to the only hole transition that has a zero minimum in the InAs QW region. Examining the hole probability densities in the InAs QW region: hh3 has the largest probability density, followed by lh1, then hh1, with the aforementioned hh2 having the lowest probability density.

Figure 1(c) shows the energy dispersion in momentum space, on the left hand side is dispersion in ' kz ', the designated growth direction and on the right hand side is the in plane dispersion ' kx, y '. The inset is an expanded view of the VB dispersion, there is considerable structure which leads to resonant absorption at ' k ' values greater than zero. This is borne out in the simulated absorption profile of figure 2.

The simulated absorption for selected temperatures (4 K, black line; 75 K, red; 150 K, green; 225 K, blue; 300 K, cyan; right axis) are shown in figure 2(a). There is an expected red shift as the temperature increases from 4 to 300 K due to the thermal expansion of the lattice as the temperature increases [37]. There are 4 distinct local maxima labeled p1–p4, where peak p1 corresponds to e1-hh1 transition. The absorption increases to a maximum value at p2 due to the contribution from all four hole levels; the energy separations for p1–p2 is 31 meV which matches the energy separation between hh1 and hh3 hole levels of the simulated energy levels (see figure 1(a) inset). The absorption maxima have energy separations: p1–p2 of 31 meV, p2–p3 of 77 meV, and p3–p4 of 91 meV, irregardless of temperature.

The peaks p3 and p4 are the result of the resonant absorption related to the structure in the energy dispersion at nonzero k values (see figure 1(c) inset). The accuracy of the higher energy peaks p3 and p4 is limited considering the shallow depth of the VBO and the simulation only including the four lowest hole states. It should be noted that p4 only appears in the simulated absorption spectra and is not in either of the simulated or experimental PL spectra.

The recombination of photogenerated carriers with a carrier density of $1 \times 10^{18} \text{ cm}^{-3}$ (4 K carrier density is $4 \times 10^{17} \text{ cm}^{-3}$ for computational reasons) for the same select temperatures is plotted (open symbols, left axis) in figure 2(a). There are two well resolved peaks in the spectra, except for 4 K which only has a single peak and 75 K where a high energy shoulder emerges in the vicinity of p2. Excluding 4 K, the two peaks correspond to p1 and p2 in the absorption spectra. For a photogenerated carrier

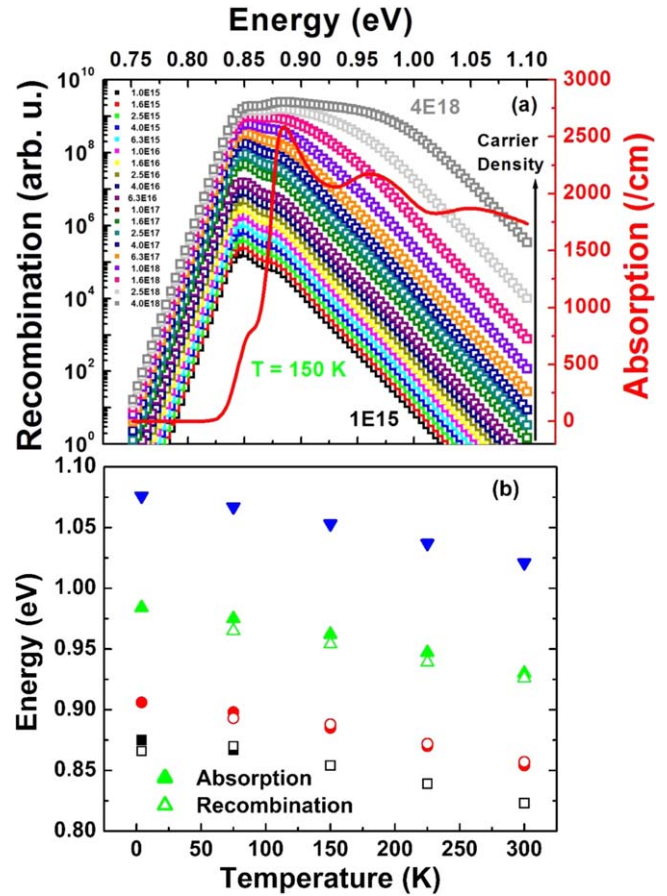


Figure 3. (a) Simulated absorption for $T = 150 \text{ K}$ (red line, right axis) and simulated recombination of photogenerated carriers as a function of carrier density (open symbols, left axis). (b) The peak energies of simulated absorption (closed symbols) and simulated recombination (open symbols) for highest carrier density simulated ($4 \times 10^{18} \text{ cm}^{-3}$, except for 4 K: $4 \times 10^{17} \text{ cm}^{-3}$).

density of $2.5 \times 10^{18} \text{ cm}^{-3}$ (figure 2(b)) p2 is also well resolved for $T = 75 \text{ K}$.

At photogenerated carrier densities $4 \times 10^{18} \text{ cm}^{-3}$ (figure 2(b)) a high energy shoulder emerges for $T = 75 \text{ K}$ and is well resolved at $T \geq 150 \text{ K}$; this high energy shoulder correlates to p3 of the simulated absorption spectra. As noted previously, the caveat for p3 and p4 in the absorption spectra applies equally to the simulated recombination spectra.

While the absorption is independent of excitation intensity, the recombination of photogenerated carriers is not. This is clearly seen in the simulated PL of figure 3(a) which shows the recombination as a power density study of the recombination as a function of energy at $T = 150 \text{ K}$. The spectra covers the range from 1×10^{15} to $4 \times 10^{18} \text{ cm}^{-3}$. Examining the peak intensity, it is not until a power density of: $2.5 \times 10^{18} \text{ cm}^{-3}$ that p2 has a greater intensity than p1; $4 \times 10^{18} \text{ cm}^{-3}$ that p3 emerges. Comparing the peak intensity of p1 and p2, the relation between temperature and power density are inversely proportional: $T = 75 \text{ K}$, p1 = p2 at $4 \times 10^{18} \text{ cm}^{-3}$; $T = 150 \text{ K}$, p2 > p1 at $2.5 \times 10^{18} \text{ cm}^{-3}$; $T = 225 \text{ K}$, p2 > p1 at $1.6 \times 10^{18} \text{ cm}^{-3}$; and $T = 300 \text{ K}$, p1 = p2 at $1 \times 10^{15} \text{ cm}^{-3}$.

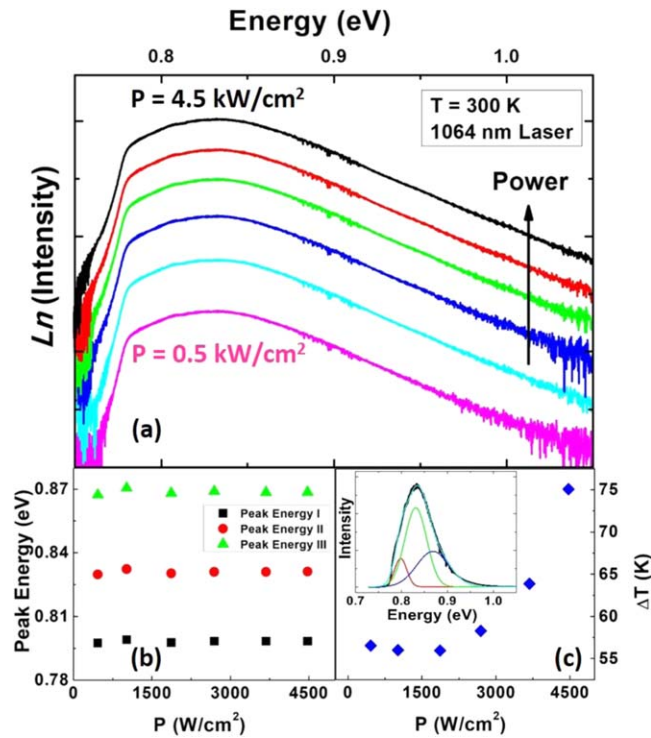


Figure 4. (a) Room temperature PL spectra as a function of power using a 1064 nm solid state laser. (b) The peak energies for a three Gaussian fit of the spectra from (a). (c) Temperature difference ΔT as a function of power. inset to (c) an example of the three Gaussian fit to spectra shown in (a) on a linear scale.

Figure 3(b) shows the peak energy of p1–p4, both for absorption (solid symbols) and for the highest ($4 \times 10^{18} \text{ cm}^{-3}$, except $4 \text{ K} - 4 \times 10^{17} \text{ cm}^{-3}$) simulated PL (open symbols) as a function of temperature. Based on the simulation results it is clear that only one peak may be observed if the temperature is low enough and the power is also low, which is the case at $T = 4 \text{ K}$ for the whole range simulated $1 \times 10^{15} - 4 \times 10^{17} \text{ cm}^{-3}$. However, at elevated temperatures the power density would have to be even less than what has been simulated for there only to be one peak.

Until $T = 225 \text{ K}$, there are only two peaks observed for a power density of $1 \times 10^{18} \text{ cm}^{-3}$ (figure 2(a)); while for a power density of $4 \times 10^{18} \text{ cm}^{-3}$, there is a hint of p3 at $T = 75 \text{ K}$, notice the discrepancy in peak energy for the absorption (solid green triangle) versus the recombination (open green triangle). Only for $T = 300 \text{ K}$ do the peak positions nearly overlap, this is due to all three peaks being clearly resolved and with the highest energy peak (p3) fully emerged; while at lower temperatures no more than 2 of the peaks are clearly resolved with highest peak (p2 $T \leq 75 \text{ K}$ or p3 $150 - 225 \text{ K}$) emerging.

It should be noted that the p2–p3 separation (77 meV) is greater than the VBO (63 meV) (figure 1(a)) for all temperatures and that the simulation only considers the lowest four hole states—overlooking the direct transition from InAs VB continuum to e1. This direct transition provides an additional recombination/absorption path that is not included in the absorption or recombination simulated data.

The natural logarithm of the peak PL intensity versus energy is shown in figure 4(a) as a function of excitation power for the 1064 nm laser at room temperature. A linear fit to the high energy tail enables the extraction of the ‘hot’ carrier temperature when using a generalized Planck relation: [9, 10, 18–23]

$$I_{\text{PL}}(E) = \frac{A(E)E^2}{4\pi^2\hbar^3c^2} \left[\exp\left(\frac{E - \Delta\mu}{k_B T_c}\right) - 1 \right]^{-1}, \quad (1)$$

where I is the PL intensity, $A(E)$ is the absorptivity as a function of energy, k_B is Boltzmann’s constant, \hbar is the reduced Planck’s constant, c is the speed of light, T_c represents the carrier temperature which can be extracted from the slope of the natural logarithm of the PL spectrum, and $\Delta\mu$ is the chemical potential. A T_c that is greater than the lattice temperature (T_L) would be considered ‘hot’; a convenient parameter is the temperature difference, ΔT ($\Delta T = T_c - T_L$).

The experimental spectra were fit using three Gaussians (see inset to figure 4(c)) to reasonably fit the entire PL spectrum, the distortion below 0.78 eV is due to detector cut-off. The extracted peak energies are plotted in figure 4(b). The lowest energy peak (p1) is 798 meV, p2 is 831 meV, and p3 is 868 meV, which correspond to e1-hh1, e1-hh3, and e1-InAs band edge transitions, respectively (see figure 1(a)). The p1–p2 energy separation is 33 meV and the p2–p3 energy separation is 37 meV. The energy separation between e1 and e2 in the CB is 655 meV (see figure 1) and therefore a transition from e2 to any lower energy state falls outside of the experimentally observed spectra. It is clear that while the e2 state is not involved in any of the observed PL spectra, higher order states in the VB do come into play.

Even with using three Gaussians to fit the spectra (see inset to figure 4(c)) the high energy tail is not fit particularly well, the PL spectra (black) is greater than the combined Gaussian fit (cyan). This is to be expected if there are hot carriers in the system. While the VB higher order states add structure to the spectra, it is still possible to apply the Boltzmann distribution to the high energy side of the spectra—where I_{PL} is nearly equal to $\varepsilon(E) \cdot \exp(-E/k_B T_c)$; here, $\varepsilon(E)$ is emissivity. When the emissivity is constant as a function of energy, then I_{PL} is proportional to $\exp(-E/k_B T_c)$ [10, 18, 19]. As reported previously in [30], that is the case for this MQW structure. Then, a linear fit of the high energy portion of the spectra shown in figure 4(a) will yield an extracted carrier temperature, T_c . It should be noted that the e1-hh1 (p1) and e1-hh3 (p2) peak positions fall outside of (below 0.87 eV) the linear portion of the high energy spectra.

Figure 4(c) is a plot of ΔT versus laser excitation power extracted from the spectra of figure 4(a) using a linear fit of the high energy tail (portion of the PL spectra beyond p3: $>868 \text{ meV}$) based on equation (1). Initially (3 lowest powers) ΔT remains relatively constant followed by a nonlinear increase in ΔT as the excitation power increases. This nonlinear increase is correlated to the extension of the PL spectra to higher energy. After a close examination of the spectra in figure 4(a), it is observed that as the power increases the

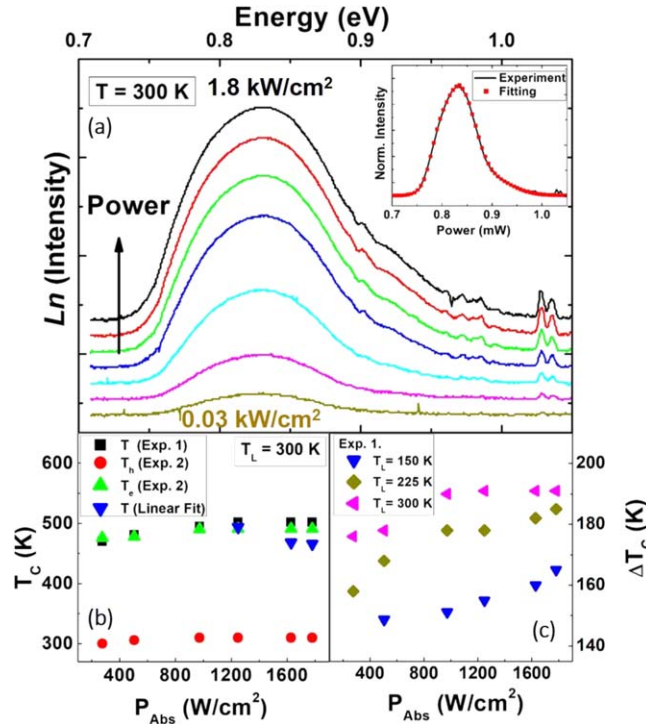


Figure 5. (a) Room temperature PL spectra as a function of power using the 633 nm line of a He–Ne laser, the inset shows the fit using equation (2) on one of the spectra with a linear scale. (b) The carrier temperature T_c using equations (1), (2), and a linear approximation of the spectra from (a). (c) Temperature difference ΔT extracted using equation (1) as a function of power for $T = 150$ K (blue symbols); 225 K (olive symbols); and 300 K (magenta symbols).

spectra extends in energy (>1 eV); for the 3 lowest powers the spectra is relatively noisy above 1 eV, while it is clear that for the highest power the spectrum is still relatively ‘clean’ out to 1.05 eV.

It is not always so straight forward to evaluate the slope of the natural logarithm of the peak PL intensity of the PL spectra, the power dependent PL spectra of the InAs MQW absorber being excited with a 632.8 nm line of a He–Ne laser is shown in figure 5(a) (the fit using equation (2) is shown in the inset). There is not a single slope associated with the high energy portion of the spectra. As previously reported [32] occupation of higher energy states affects the extracted temperature and is not necessarily representative of a hot carrier temperature but, rather a temperature associated with the convolution of overlapping energy states. Following the methodology from Gibelli *et al* [29] the PL intensity is described with the non equilibrium generalized Planck relation:

$$I_{\text{PL}}(E) = \frac{A(E)E^2}{4\pi^2\hbar^3c^2} \left[\exp\left(\frac{1}{k_B}\left(\frac{1}{T_e} - \frac{1}{T_h}\right)\right) \times \left[\left(\frac{m_e}{m_e + m_h}\right)\left(\frac{E_g}{2} + E_c\right) - \left(\frac{m_h}{m_e + m_h}\right)\left(\frac{E_g}{2} + E_v\right) \right] + \frac{\hbar\omega}{k_B(m_e + m_h)}\left(\frac{m_h}{T_e} + \frac{m_e}{T_h}\right) - \frac{\mu_e}{k_B T_e} - \frac{\mu_h}{k_B T_h} - 1 \right]^{-1}. \quad (2)$$

Now, instead of a single carrier temperature, T_c , electrons (holes) have their own associated temperature and chemical potential: T_e and μ_e (T_h and μ_h). E_g , E_c , and E_v are the energies of the band gap, CB, and VB, respectively; m_e (m_h) is the mass of the electron (hole) and ω is the angular frequency of the photoluminescent photon. The absorptivity $A(E)$ is a function of energy, this model ([29]) has three energy level transitions: two from VB levels (light hole and heavy hole) and a transition to the continuum. With regards to the InAs MQW structure, the two VB levels modeled are associated with e1-hh1 and e1-hh3 and the transition to the continuum is associated with e1-InAs VB edge states.

The extracted carrier temperature for the spectra of figure 5(a) is shown in figure 5(b). The carrier temperature has been determined by three different methods: (1) a full spectrum fit using equation (1) (T_c , black squares); (2) a full spectrum fit using equation (2) (T_h for holes, red circles; T_e for electrons, green triangles); and (3) a linear fit of the high energy portion of the PL spectra (T , blue triangles, where the high energy portion was broken into two separate regions). Due to the convolution of higher energy states affecting the extracted carrier temperature for the spectra at low powers, only the extracted carrier temperature of the three highest powers are included for the linear fit (for the region from 875 to 900 meV).

Not only do the individual extracted hot carrier temperatures for the linear fit (T , blue triangles) and equation (1) (T_c , black squares) yield similar results but, the electron temperature, (T_e), of equation (2) *also* yields a comparable carrier temperature: T_c —black squares (equation (1)) and T_e —green triangles (equation (2)) overlap. The carrier temperature for holes, T_h , is only slightly hotter than the lattice temperature, ($T_L = 300$ K); the hole temperature being nearly equal to the T_L is not at all surprising considering the hole state separation (see inset figure 1(a)) is on the order of both the LO phonon energy (AlAsSb ~ 44 meV) and $k_B T$ (26 meV).

The temperature difference, ΔT , extracted from the full spectrum fit using equation (1) is shown in figure 5(c) for three different temperatures: $T = 150$ K (blue triangles), 225 K (olive diamonds), and 300 K (magenta triangles). Remarkably, ΔT increases as the T_L increases, this is attributed to the delocalization of holes and the emergence of the ‘ideal’ type-II band alignment at elevated temperatures, as reported previously [18, 30]. The simulated results serve as additional confirmation of the hole delocalization with the VBO of 63 meV (see inset figure 1(a)) being not much more than twice $k_B T$ (52 meV); therefore, holes will have sufficient energy to move throughout the VB. Also, the small separation of hole states allows for efficient thermalization of any ‘hot’ holes [21–23, 31].

As to how all three methods result in similar temperatures, the basis for that stems from each method starting with the generalized Planck relation for radiative recombination, equation (1). Both, a full spectrum fit using equation (1) or applying a linear fit only to the high energy portion have a single carrier temperature which would describe holes, as well as,

electrons. Whereas, equation (2) has individual temperatures associated with electrons and holes. Due to the small energy separation of hole levels (30–40 meV) it is probably much more realistic to consider separate carrier temperatures as evaluated using equation (2), which results in slightly hot holes (T_h) and hot electrons (T_e) comparable to the other methods. Worth mentioning but not shown for clarity purposes, is that a three Gaussian fit of figure 5 spectra yields similar values for p1 and p2 with a slightly higher value for e1-InAs VB edge continuum; this slightly higher value (~20 meV higher) is most likely due to greater absorption of the shorter wavelength excitation leading to higher occupancy of the continuum states.

Comparing the experimental spectra to the simulated spectra, the lowest energy peak (p1) is 798 meV for the experimental data and 805 meV for the simulated. The p1–p2 energy separations are 33 meV (exp) and 31 meV (sim); p2–p3 experimental energy separation is 37 meV compared to 77 meV simulated. As previously noted the InAs VB continuum to e1 transition is not included in the simulation and a p2 to InAs VB separation would be 26 meV for the simulation. With the experimental p1 actually being 7 meV smaller than the simulation that would correspond to a greater VBO than the simulation; i.e., a VBO of 70 meV rather than 63 meV, with a corresponding increase of the p2-InAs VB separation to 33 meV rather than 26 meV. The experimental spectrum has quenched in the p4 region of the simulation.

In summary, NRL's MultiBands[®] simulations describe the actual PL spectra of the InAs/AlAsSb MQW hot carrier absorber. In particular, the e1-hh1 simulated transition energy of 805 meV closely matches the 798 meV transition energy of the experimental PL spectra, a difference of only 7 meV. Likewise, the expected energy separations between p1 and p2 have a difference of just 2 meV: a simulated separation of 31 meV compared to the experimental value of 33 meV. The main difference is in the energy separation between p2 and p3 but, that is accounted for by the InAs VB continuum to e1 transition not being included in the simulated data. Moreover, the simulated band structure would correlate to a comparable energy transition when accounting for the difference in measured and simulated results: an adjusted InAs VB continuum to e1 simulated transition of 33 meV corresponds to an experimental value of 37 meV, with a difference of only 4 meV.

Backed by a more thorough understanding of the VB structure provided by the simulated data, the high energy portion of the experimental spectra can be confidently evaluated. The close spacing (less than 33 meV) in the lowest four VB states allows for efficient thermalization (LO phonon energy 44 meV; $k_B T$ 26 meV). Furthermore, utilizing a non equilibrium generalized Planck relation a full spectrum fit enables individual carrier temperatures for both holes and electrons. This results in two very different carrier temperatures for holes and electrons, where T_h is nearly equal to T_L , while T_e is 'hot'. Also, by fitting the experimental spectra via three different methods a 'hot' carrier temperature is associated with *electrons only*; all three methods yield similar 'hot' carrier temperatures. This observation suggest that

narrow gap heterostructures [38, 39] could be a good candidate for hot carrier absorbers [12, 33, 40, 41].

Acknowledgments

The authors acknowledge financial support from the National Science Foundation (NSF), through the ECCS program: ECCS# 1610062 and through Grant No. DMR-1229678 in the acquisition of the GENxplor MBE system; the Department of Energy through: DURIP2016 Program, 16RT0183; and the US Air Force Office of Scientific Research (AFOSR) under grants FA9550-14-1-037 and FA9550-17-1-0341. The GENxplor MBE system was acquired with support from the NSF through Grant No. DMR-1229678.

References

- [1] Chapin D M, Fuller C S and Pearson G L 1954 *J. Appl. Phys.* **25** 676
- [2] Klemens P G 1966 *Phys. Rev.* **148** 845
- [3] Shah J, Pinczuk A, Störmer H L, Gossard A C and Wiegmann W 1983 *Appl. Phys. Lett.* **42** 55
- [4] Hirst L C and Ekins-Daukes N J 2010 *Prog. Photovolt., Res. Appl.* **19** 286
- [5] Shockley W and Queisser H J 1961 *J. Appl. Phys.* **32** 510
- [6] Chiu P T *et al* 2014 *2014 IEEE 40th Photovoltaic Specialist Conf. (PVSC)* pp 0011–3
- [7] Pötz W and Kocevar P 1983 *Phys. Rev. B* **28** 7040
- [8] Clady R, Tayebjee M J Y, Aliberti P, König D, Ekins-Daukes N J, Conibeer G J, Schmidt T W and Green M A 2011 *Prog. Photovolt., Res. Appl.* **20** 82
- [9] Hirst L C *et al* 2014 *IEEE J. Photovolt.* **4** 244
- [10] Le Bris A *et al* 2012 *Energy Environ. Sci.* **5** 6225
- [11] Hirst L C *et al* 2014 *Appl. Phys. Lett.* **104** 231115
- [12] Farrell D J, Takeda Y, Nishikawa K, Nagashima T, Motohiro T and Ekins-Daukes N J 2011 *Appl. Phys. Lett.* **99** 111102
- [13] Conibeer G *et al* 2009 *Sol. Energy Mater. Sol. Cells* **93** 713
- [14] Dimmock J A R, Day S, Kauer M, Smith K and Heffernan J 2014 *Prog. Photovolt., Res. Appl.* **22** 151
- [15] Landsberg P T and Markvart T 1998 *Solid-State Electron.* **42** 657
- [16] Cebulla U *et al* 1988 *Solid-State Electron.* **31** 507
- [17] Shah J *et al* 1986 *Surf. Sci.* **174** 363
- [18] Tang J, Whiteside V, Esmailpour H, Vijayaragunathan S, Mishima T, Santos M and Sellers I 2015 *Appl. Phys. Lett.* **106** 061902
- [19] Hirst L C, Yakes M K, Bailey C G, Tischler J G, Lumb M P, González M, Fuhrer M F, Ekins-Daukes N and Walters R J 2014 *IEEE J. Photovolt.* **4** 1526
- [20] Balkan N, Ridley B, Emeny M and Goodridge I 1989 *Semicond. Sci. Technol.* **4** 852
- [21] Rosenwaks Y, Hanna M, Levi D, Szymyd D, Ahrenkiel R and Nozik A 1993 *Phys. Rev. B* **48** 14675
- [22] Shah J, Pinczuk A, Gossard A and Wiegmann W 1985 *Phys. Rev. Lett.* **54** 2045
- [23] Leo K, Rühle W and Ploog K 1988 *Phys. Rev. B* **38** 1947
- [24] Nelson J, Barnes J, Ekins-Daukes N, Klufftinger B, Tsui E, Barnham K, Foxon C T, Cheng T and Roberts J S 1997 *J. Appl. Phys.* **82** 6240

- [25] Bessiere A, Connolly J P, Barnham K W J, Ballard I M, Mazzer M, Johnson D C, Hill G and Roberts J S 2005 *Proc 20th European Photovoltaic Solar Energy Conf.*
- [26] Fuhrer M F, Bessiere A, Ballard I M, Johnson D C, Mazzer M, Barnham K W J, Roberts J S, Airey R and Calder C 2006 *Proc 21st European Photovoltaic Solar Energy Conf.*
- [27] Fuhrer M F, Connolly J P, Mazzer M, Ballard I M, Johnson D C, Barnham K W J, Bessiere A, Roberts J S, Airey R and Calder C 2007 *Proc 22nd European Photovoltaic Solar Energy Conf.*
- [28] Fuhrer M F *et al* 2008 *2008 33rd IEEE Photovoltaic Specialists Conf.* pp 1–5
- [29] Gibelli F, Lombez L and Guillemoles J-F 2017 *J. Phys.: Condens. Matter* **29** 06LT02
- [30] Esmailpour H, Whiteside V R, Tang J, Vijayaragunathan S, Mishima T D, Cairns S, Santos M B, Wang B and Sellers I R 2016 *Prog. Photovolt., Res. Appl.* **24** 591
- [31] Benisty H, Sotomayor-Torrès C M and Weisbuch C 1991 *Phys. Rev. B* **44** 10945
- [32] Esmailpour H, Whiteside V R, Hirst L C, Tischler J G, Ellis C T, Lumb M P, Forbes D V, Walters R J and Sellers I R 2017 *Prog. Photovolt., Res. Appl.* **25** 782
- [33] König D, Takeda Y and Puthen-Veetil B 2012 *Appl. Phys. Lett.* **101** 153901
- [34] Esmailpour H *et al* 2018 *Sci. Rep.* **8** 12473
- [35] Lumb M P, Vurgaftman I, Affouda C A, Meyer J R, Aifer E H and Walters R J 2012 *Proc. SPIE* **8471** 8471
- [36] Vurgaftman I, Meyer J R and Ram-Mohan L R 2001 *J. Appl. Phys.* **89** 5815
- [37] Varshni Y 1967 *Physica* **34** 149
- [38] Bhowmick M, Khodaparast G A, Mishima T D, Santos M B, Saha D, Sanders G and Stanton C J 2016 *J. Appl. Phys.* **120** 235702
- [39] Meeker M A, Magill B A, Merritt T R, Bhowmick M, McCutcheon K, Khodaparast G A, Tischler J G, McGill S, Choi S G and Palmstrøm C J 2013 *Appl. Phys. Lett.* **102** 222102
- [40] Hanna M C and Nozik A J 2006 *J. Appl. Phys.* **100** 074510
- [41] Aliberti P, Feng Y, Takeda Y, Shrestha S K, Green M A and Conibeer G 2010 *J. Appl. Phys.* **108** 094507